

# $M1$ resonance in $^{208}\text{Pb}$ within the self-consistent phonon-coupling model

V. Tselyaev\* and N. Lyutorovich

*St. Petersburg State University, St. Petersburg, 199034, Russia*

J. Speth

*Institut für Kernphysik, Forschungszentrum Jülich, D-52425 Jülich, Germany*

P.-G. Reinhard

*Institut für Theoretische Physik II, Universität Erlangen-Nürnberg, D-91058 Erlangen, Germany*

(Dated: October 8, 2020)

The main goal of the paper is to investigate theoretically the experimentally observed fragmentation of the isovector  $M1$  resonance in  $^{208}\text{Pb}$  within a self-consistent model based on an energy-density functional (EDF) of the Skyrme type. This fragmentation (spread of the  $M1$  strength) is not reproduced in a conventional one-particle–one-hole ( $1p1h$ ) random-phase approximation (RPA) and thus has to be investigated in the framework of more complicated models. However, previously applied models of this type were not self-consistent. In the present work, we use a recently developed renormalized version of the self-consistent time blocking approximation (RenTBA) in which the  $1p1h\otimes$ phonon configurations are included on top of the RPA  $1p1h$  configurations. We have determined several sets of the parameters of the modified Skyrme EDF fitted within the RenTBA and RPA and have found the necessary condition of producing the fragmentation of the  $M1$  resonance in  $^{208}\text{Pb}$  in our model. We present also the results of the RenTBA and RPA calculations for the first excited states of the natural parity modes in  $^{208}\text{Pb}$  obtained with these modified parametrizations.

## I. INTRODUCTION

Magnetic dipole ( $M1$ ) excitations in the  $^{208}\text{Pb}$  nucleus are the object of numerous experimental and theoretical investigations for several decades. From the theoretical point of view, one of the reasons is the possibility of determining the spin-related parameters of the residual interaction in the calculations of these excitations within the random-phase approximation (RPA) or its extended versions. The calculated energies of the unnatural parity excitations are very sensitive to the values of the underlying model parameters, in particular, of the parameters of the Skyrme energy-density functional. The comparison of these energies with experimental data is the only reliable method to estimate the spin-related parameters of the model. Another reason is the fragmentation (spread) of the isovector  $M1$  resonance in  $^{208}\text{Pb}$  which is observed in the experiment (see [1]) but which is absent in RPA where the isovector  $M1$  strength in this nucleus is concentrated in one state. The description of this fragmentation requires application of more complicated models going beyond the RPA framework (see, e.g., Ref. [2] for more details).

Most of the early calculations of the  $M1$  excitations in  $^{208}\text{Pb}$  (see, e.g., Refs. [3–7]) were performed within the RPA, the Tamm-Dancoff approximation or within the Migdal’s Theory of Finite Fermi Systems (TFFS, Ref. [8]) which in its simplest form used in the applications is equivalent to the RPA with the zero-range residual interaction. In the following, the  $M1$  modes were investigated within the generalized models in which the one-particle–one-hole ( $1p1h$ ) RPA configuration space is enlarged by adding  $2p2h$ ,  $1p1h\otimes$ phonon or two-phonons configurations (see, e.g., [9–17]). However, the fully self-consistent calculations of the  $M1$  excitations in  $^{208}\text{Pb}$  have been performed so far only within the RPA (see Refs. [18–23]).

In a broad sense, self-consistency means the use of the same energy-density functional (EDF)  $E[\rho]$  (where  $\rho$  is the single-particle density matrix) for the mean field as well as for the RPA residual interaction. This decreases the number of the free parameters of the theory and, in principle, increases its predictive power. Here we use an EDF of Skyrme type [24]. In a recent paper [23], we have shown that the adequate description of the low-energy  $M1$  excitations in  $^{208}\text{Pb}$  within the self-consistent RPA based on the Skyrme EDF is possible only if the spin-related parameters of the known EDF are modified. By re-tuning these parameters we managed to reproduce

---

\* tselyaev@mail.ru

within the RPA the experimental key quantities: energy and the strength of the  $1_1^+$  state as well as the mean energy and the summed strength of the  $M1$  resonance in  $^{208}\text{Pb}$  in the interval 6.6-8.1 MeV. However, as mentioned above, the observed fragmentation of the isovector  $M1$  resonance and its total width in this model are not yet reproduced.

The aim of the present paper is to study the possibility to describe this fragmentation within the extended self-consistent model including the  $1p1h \otimes$  phonon configurations on top of the RPA  $1p1h$  configurations. This extended model is treated within the time blocking approximation (TBA) which we use actually in its renormalized version (RenTBA, [25]). Full self-consistency is maintained also for the extended treatment. The method of re-tuning the spin-related parameters of the Skyrme EDF developed in Ref. [23] is used also for the RenTBA.

The paper is organized as follows. In Section II the formalism of RPA and RenTBA is briefly described. Section III contains the numerical details and the calculation scheme. The main results of the paper are presented in Section IV. In Section V the fine structure of the  $M1$  strength distributions in  $^{208}\text{Pb}$  and the impact of the single-particle continuum on this structure are analyzed. In Section VI the problem of the fragmentation of the isovector  $M1$  resonance in  $^{208}\text{Pb}$  is discussed in detail and the necessary condition of the description of this fragmentation is determined. In Section VII we present the results of the RenTBA and RPA calculations of the low-energy electric excitations in  $^{208}\text{Pb}$  obtained with the use of the modified parametrizations of the Skyrme EDF. The conclusions are given in the last section.

## II. THE MODEL

Let us start with the RPA eigenvalue equation

$$\sum_{34} \Omega_{12,34}^{\text{RPA}} Z_{34}^n = \omega_n Z_{12}^n, \quad (1)$$

where  $\omega_n$  is the excitation energy,  $Z_{12}^n$  is the transition amplitude, and the numerical indices  $(1, 2, 3, \dots)$  stand for the sets of the quantum numbers of some single-particle basis. In what follows the indices  $p$  and  $h$  are used to label the states of the particles and holes in the basis which diagonalizes the single-particle density matrix  $\rho$  and the single-particle Hamiltonian  $h$  in the ground state [see Eq. (5) below]. The transition amplitudes are

normalized by the condition

$$\langle Z^n | M^{\text{RPA}} | Z^n \rangle = \text{sgn}(\omega_n), \quad (2)$$

where

$$M_{12,34}^{\text{RPA}} = \delta_{13} \rho_{42} - \rho_{13} \delta_{42} \quad (3)$$

is the metric matrix in the RPA.

In the self-consistent RPA based on the EDF  $E[\rho]$  the RPA matrix  $\Omega^{\text{RPA}}$  is defined by

$$\Omega_{12,34}^{\text{RPA}} = h_{13} \delta_{42} - \delta_{13} h_{42} + \sum_{56} M_{12,56}^{\text{RPA}} V_{56,34}, \quad (4)$$

where the single-particle Hamiltonian  $h$  and the amplitude of the residual interaction  $V$  are linked by the relations

$$h_{12} = \frac{\delta E[\rho]}{\delta \rho_{21}}, \quad V_{12,34} = \frac{\delta^2 E[\rho]}{\delta \rho_{21} \delta \rho_{34}}. \quad (5)$$

In the TBA, the counterpart of Eq. (1) has the form

$$\sum_{34} \Omega_{12,34}^{\text{TBA}}(\omega_\nu) z_{34}^\nu = \omega_\nu z_{12}^\nu, \quad (6)$$

where

$$\Omega_{12,34}^{\text{TBA}}(\omega) = \Omega_{12,34}^{\text{RPA}} + \sum_{56} M_{12,56}^{\text{RPA}} \bar{W}_{56,34}(\omega), \quad (7a)$$

$$\bar{W}_{12,34}(\omega) = W_{12,34}(\omega) - W_{12,34}(0). \quad (7b)$$

The matrix  $\Omega^{\text{TBA}}(\omega)$  is energy-dependent due to the matrix  $W(\omega)$  which represents the induced interaction generated by the intermediate  $1p1h \otimes$  phonon configurations. The subtraction of  $W(0)$  in Eq. (7b) serves to avoid changing the mean-field ground state [26, 27] and to ensure stability of solutions of the TBA eigenvalue equation (see [28]). The matrix  $W(\omega)$  is defined by the equations

$$W_{12,34}(\omega) = \sum_{c, \sigma} \frac{\sigma F_{12}^{c(\sigma)} F_{34}^{c(\sigma)*}}{\omega - \sigma \Omega_c}, \quad (8a)$$

$$\Omega_c = \varepsilon_{p'} - \varepsilon_{h'} + \omega_\nu, \quad \omega_\nu > 0, \quad (8b)$$

where  $\sigma = \pm 1$ ,  $c = \{p', h', \nu\}$  is a combined index for the  $1p1h \otimes$  phonon configurations,  $\nu$  is the phonon's index,  $\varepsilon_{p'}$  and  $\varepsilon_{h'}$  are the particle's and hole's energies,  $\omega_\nu$  is the phonon's energy. The amplitudes  $F_{12}^{c(\sigma)}$  have only particle-hole matrix elements  $F_{ph}^{c(\sigma)}$  and  $F_{hp}^{c(\sigma)}$ . They are defined by the equations

$$F_{12}^{c(-)} = F_{21}^{c(+)*}, \quad F_{ph}^{c(-)} = F_{hp}^{c(+)} = 0, \quad (9a)$$

$$F_{ph}^{c(+)} = \delta_{pp'} g_{h'h}^\nu - \delta_{h'h} g_{pp'}^\nu, \quad (9b)$$

where  $g'_{12}$  is an amplitude of the quasiparticle-phonon interaction.

In the conventional TBA, the phonon's energies  $\omega_\nu$  in Eq. (8b) and the amplitudes  $g'_{12}$  in Eq. (9b) are determined within the framework of the RPA. In the non-linear version of the TBA developed in Ref. [25], the phonon's energies  $\omega_\nu$  are the solutions of the TBA equation (6), while the amplitudes  $g'_{12}$  are expressed through the transition amplitudes  $z'_{12}$  which are also the solutions of Eq. (6), namely

$$g'_{12} = \sum_{34} V_{12,34} z'_{34}. \quad (10)$$

The normalization condition for the transition amplitudes  $z'_{12}$  has the form

$$(z'_{12})_{\text{RPA}}^2 + (z'_{12})_{\text{CC}}^2 = 1, \quad (11)$$

where

$$(z'_{12})_{\text{RPA}}^2 = \text{sgn}(\omega_\nu) \langle z'_{12} | M^{\text{RPA}} | z'_{12} \rangle, \quad (12a)$$

$$(z'_{12})_{\text{CC}}^2 = -\text{sgn}(\omega_\nu) \langle z'_{12} | W'_\nu | z'_{12} \rangle, \quad (12b)$$

$$W'_\nu = \left( \frac{dW(\omega)}{d\omega} \right)_{\omega=\omega_\nu}. \quad (12c)$$

The terms  $(z'_{12})_{\text{RPA}}^2$  and  $(z'_{12})_{\text{CC}}^2$  represent the contributions of the  $1p1h$  components (RPA) and of the complex configurations (CC) to the norm (11). The model includes only those TBA phonons that satisfy the condition

$$(z'_{12})_{\text{RPA}}^2 > (z'_{12})_{\text{CC}}^2, \quad (13)$$

which together with Eq. (11) means that

$$(z'_{12})_{\text{RPA}}^2 > \frac{1}{2}. \quad (14)$$

The condition (13) confines the phonon space to the RPA-like phonons in agreement with the basic model approximations.

The feedback described above renders the phonon space of RenTBA fully self-consistent. In the present paper we use the version of this non-linear model in which the energies  $\omega_\nu$  and the amplitudes  $z'_{12}$  entering Eqs. (8b) and (10) (and only in these equations) are determined from the solutions of the TBA equation (6) in the diagonal approximation. This model is what we call the renormalized TBA (RenTBA, see [25] for more details).

### III. NUMERICAL DETAILS AND THE CALCULATION SCHEME

The equations of RPA and RenTBA were solved within the fully self-consistent scheme as described in Refs. [29–31]. Wave functions and fields were represented on a spherical grid in coordinate space. The single-particle basis was discretized by imposing the box boundary condition with the box radius equal to 18 fm. The particle's energies  $\varepsilon_p$  were limited by the maximum value  $\varepsilon_p^{\text{max}} = 100$  MeV. The non-linear RenTBA equations were solved by means of the iterative procedure. The phonon space of the first iteration included the RPA phonons with the energies  $\omega_n \leq 50$  MeV and multiplicities  $L \leq 15$  of both the electric and magnetic types which have been selected according to the criterion of collectivity

$$\langle Z^n | V^2 | Z^n \rangle / \omega_n^2 \geq 0.05, \quad (15)$$

see [25].

The field operator  $\mathbf{Q}$  in the case of the  $M1$  excitations was taken in the form

$$\mathbf{Q} = \mu_N \sqrt{\frac{3}{16\pi}} \left\{ (\gamma_n + \gamma_p) \boldsymbol{\sigma} + \mathbf{l} + [(1 - 2\xi_s)(\gamma_n - \gamma_p) \boldsymbol{\sigma} - (1 - 2\xi_l) \mathbf{l}] \tau_3 \right\} \quad (16)$$

where  $\mathbf{l}$  is the single-particle operator of the angular momentum,  $\boldsymbol{\sigma}$  and  $\tau_3$  are the spin and isospin Pauli matrices, respectively (with positive eigenvalue of  $\tau_3$  for the neutrons),  $\mu_N = e\hbar/2m_p c$  is the nuclear magneton,  $\gamma_p = 2.793$  and  $\gamma_n = -1.913$  are the spin gyromagnetic ratios,  $\xi_s$  and  $\xi_l$  are the renormalization constants. The nonzero  $\xi_s$  and  $\xi_l$  correspond to the effective operator  $\mathbf{Q}$ , however in the present calculations we used  $\xi_l = 0$ . Thus, the reduced probability of the  $M1$  excitations  $B(M1)$  is defined as  $|\langle Z^n | \mathbf{Q} \rangle|^2$  in the RPA and as  $|\langle z'_{12} | \mathbf{Q} \rangle|^2$  in the RenTBA.

The Skyrme EDF with the basis parametrizations SKXm [32] and SV-bas [33] was used both in RPA and RenTBA. The nuclear matter parameters for these parametrizations are listed in Table I.

There are four experimental characteristics of the  $M1$  excitations in  $^{208}\text{Pb}$  which serve as a benchmark in our calculations: energy and excitation probability of the isoscalar  $1_1^+$  state ( $E_1 = 5.84$  MeV with  $B_1(M1) = 2.0 \mu_N^2$ , see [34]) and the mean energy and the summed strength of the isovector  $M1$  resonance in the interval 6.6–8.1 MeV ( $E_2 = 7.4$  MeV with  $B_2(M1) = \sum B(M1) = 15.3 \mu_N^2$ ). The latter two quantities have been deduced by combining the data from Refs. [34, 35].

TABLE I. Nuclear matter parameters: effective mass  $m^*/m$ , incompressibility  $K_\infty$ , Thomas-Reiche-Kuhn sum rule enhancement factor  $\kappa_{\text{TRK}}$ , and symmetry energy  $a_{\text{sym}}$  for two Skyrme-EDF parametrizations: SKXm [32] and SV-bas [33].

EDF	$m^*/m$	$K_\infty$ (MeV)	$\kappa_{\text{TRK}}$	$a_{\text{sym}}$ (MeV)
SKXm	0.97	238	0.34	31
SV-bas	0.90	233	0.40	30

To reproduce these key characteristics, the spin-related EDF parameters  $W_0$  (spin-orbit strength),  $x_W$  (proton-neutron balance of the spin-orbit term),  $g$  (Landau parameter for isoscalar spin mode), and  $g'$  (Landau parameter for isovector spin mode) were refitted as explained in [23] while the remaining spin-related parameters of the functional were switched off. The values of all other parameters of the functional were kept at the values of the original parametrizations. The form of the EDF containing all the parameters mentioned above is given in Ref. [23]. The spin-orbit parameters  $x_W$  and  $W_0$  were refitted to reproduce the experimental value of  $B_1(M1)$ . The parameters  $g$  and  $g'$  enter the terms of the modified Skyrme EDF which yield the term  $V^s$  of the residual interaction  $V$  having the form of the Landau-Migdal ansatz

$$V^s = C_N (g \boldsymbol{\sigma} \cdot \boldsymbol{\sigma}' + g' \boldsymbol{\sigma} \cdot \boldsymbol{\sigma}' \boldsymbol{\tau} \cdot \boldsymbol{\tau}'), \quad (17)$$

where  $C_N$  is the normalization constant. These parameters allow us to change the calculated energies of the isoscalar and isovector  $1^+$  states.

Note that the parameter  $x_W$  was introduced in Refs. [36, 37] (with the use of slightly different notations in [36]) to regulate the isospin dependence of the spin-orbit potential. In the most parametrizations of the Skyrme EDF the value  $x_W \geq 0$  is used (see, e.g., last two lines of Table II). In particular, the value  $x_W = 1$  (frequently used implicitly) corresponds to the usual Hartree-Fock approximation in the EDF for the two-body spin-orbit zero-range interaction. However, in all these cases the value of  $B_1(M1)$  in  $^{208}\text{Pb}$  calculated within the fully self-consistent RPA is much larger than its experimental value  $B_1(M1)_{\text{exp}} = 2.0 \mu_N^2$ . For instance,  $B_1(M1)_{\text{RPA}} \approx 10 B_1(M1)_{\text{exp}}$  for the SLy5 set [38] even with the use of the effective  $M1$  operator (16). In Ref. [23] we have shown that one should use the negative values of  $x_W$  to decrease the calculated  $B_1(M1)$  up to  $B_1(M1)_{\text{exp}}$ . The values of the parameter  $W_0$  should be simultaneously increased because from the set of the refitted parameters

$x_W$ ,  $W_0$ ,  $g$ , and  $g'$ , only the isoscalar combination of the spin-orbit parameters  $C_0^{\nabla J} = -\frac{1}{4}(2 + x_W)W_0$  have an impact on the ground-state characteristics of spherical nuclei (see [23] for more details). This combination remains approximately unchanged in our refitting procedure, so the quality of the description of the ground-state properties with the use of the original and modified parametrizations of the Skyrme EDF is approximately the same.

#### IV. THE MAIN RESULTS FOR THE $M1$ RESONANCE IN $^{208}\text{Pb}$

The parametrizations obtained in the result of the refitting procedure described above are SKXm $_{-0.54}$  and SV-bas $_{-0.50}$  for the RPA and SKXm $_{-0.49}$  and SV-bas $_{-0.44}$  for the RenTBA (here and in the following the numerical subindex of the modified parametrization indicates the value of the parameter  $x_W$ ). The values of the refitted parameters for these sets are shown in Table II along with several sets discussed in Sec. VI. In addition, we used the renormalization constant  $\xi_s$  in the field operator of the  $M1$  excitations (16) to fit the isovector  $M1$  strength. The values of this constant for the RPA and RenTBA are also shown in Table II.

TABLE II. Parameters  $x_W$ ,  $W_0$ ,  $g$ , and  $g'$  of the modified Skyrme EDFs determined on the basis of the parametrizations SKXm [32] and SV-bas [33]. The Landau-Migdal parameters  $g$  and  $g'$  are normalized to  $C_N = 300 \text{ MeV} \cdot \text{fm}^3$ . The renormalization constants  $\xi_s$  of the field operator of the  $M1$  excitations corresponding to the each parametrization are shown in the last column. The parameters of the original sets are shown in the last two lines.

EDF	$x_W$	$W_0$ (MeV·fm <sup>5</sup> )	$g$	$g'$	$\xi_s$
SKXm $_{-0.54}$	-0.54	226.0	-0.078	0.430	0.156
SV-bas $_{-0.50}$	-0.50	213.0	-0.028	0.516	0.156
SKXm $_{-0.49}$	-0.49	218.5	0.108	0.930	0.085
SKXm' $_{-0.49}$	-0.49	218.5	0.108	0.900	0.085
SKXm'' $_{-0.49}$	-0.49	218.5	-0.067	0.435	0.151
SV-bas $_{-0.44}$	-0.44	204.7	0.177	1.030	0.085
SV-bas' $_{-0.44}$	-0.44	204.7	0.177	1.460	0.085
SKXm	0	155.9	0	0	
SV-bas	0.55	124.6	0	0	

Note that the set of the phonons in the RenTBA after the renormalization procedure with the use of the condition (14) included 123 electric and 83 magnetic

phonons for the parametrization SKXm<sub>-0.49</sub> and 121 electric and 85 magnetic phonons for the parametrization SV-bas<sub>-0.44</sub>.

Most of the calculations presented below have been performed within the discrete versions of RPA and RenTBA that means that the model equations are solved in the discrete basis representation with the use of the box boundary conditions for all functions entering these equations. It is convenient to present these results as well as the experimental data in the form of the strength functions  $S(E)$  obtained by folding the discrete spectra with a Lorentzian of half-width  $\Delta$ :

$$S(E) = \frac{\Delta}{\pi} \sum_{\nu} \frac{\text{sgn}(\omega_{\nu}) B_{\nu}(M1)}{(E - \omega_{\nu})^2 + \Delta^2}. \quad (18)$$

The results for the modified SKXm parametrizations SKXm<sub>-0.49</sub> (RenTBA) and SKXm<sub>-0.54</sub> (RPA) obtained with  $\Delta = 20$  keV are shown on the upper panel of Fig. 1. The experimental spectra were taken from Refs. [34] [ $^{208}\text{Pb}(\gamma, \gamma')$  reaction, data below the neutron separation energy  $S(n) = 7.37$  MeV] and [35] [ $^{207}\text{Pb}(n, \gamma)$  reaction, data above  $S(n)$ ].

The RenTBA, in contrast to the RPA, reproduces the experimental splitting of the  $M1$  resonance into two components separated by the dip near 7.4 MeV. The quantitative characteristics of this splitting are given in Table III in comparison with the experiment. The experi-

TABLE III. The summed strengths  $\sum B(M1)$  and the mean energies  $\bar{E}$  of the  $M1$  excitations calculated within the RenTBA with parametrization SKXm<sub>-0.49</sub> in two energy intervals. The last column contains the Gaussian width  $\Gamma$  of the  $M1$  strength distribution calculated in the interval 6.6–8.1 MeV. The experimental data are taken from Refs. [34, 35].

interval	6.60–7.37 MeV		7.37–8.10 MeV		
	$\sum B(M1)_{<}$	$\bar{E}_{<}$	$\sum B(M1)_{>}$	$\bar{E}_{>}$	$\Gamma$
	( $\mu_N^2$ )	(MeV)	( $\mu_N^2$ )	(MeV)	(MeV)
theory	7.6	7.32	7.8	7.46	0.20
experiment	9.2	7.26	6.2	7.57	0.44

mental summed  $M1$  strength in the energy interval below the neutron threshold  $\sum B(M1)_{<}$  is greater than the strength above the threshold  $\sum B(M1)_{>}$  by about 50%, while the respective theoretical values are approximately equal to each other. Nevertheless, the total theoretical summed  $M1$  strength in the interval 6.6–8.1 MeV is equal to the experimental one according to the conditions of construction of our modified parametrizations. The absolute values of the calculated mean energies  $\bar{E}_{<}$

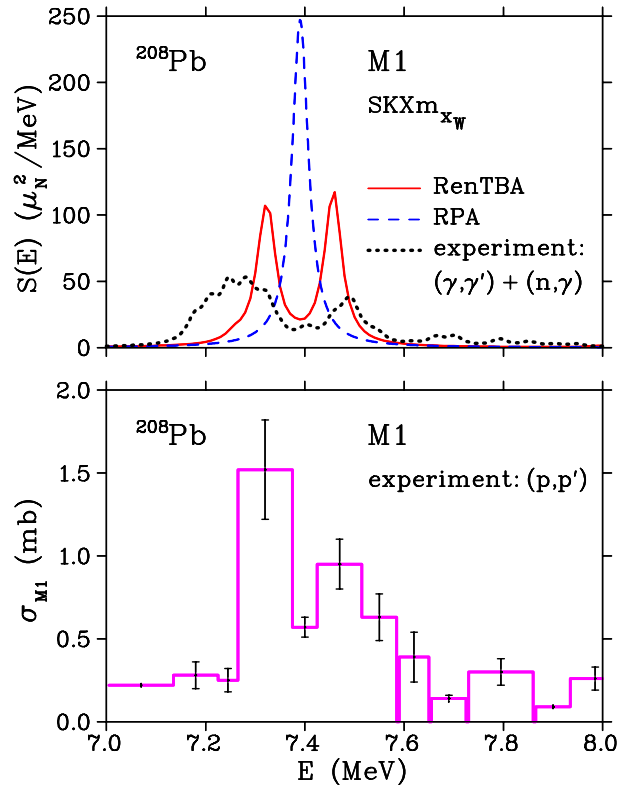


FIG. 1. Upper panel: strength distributions of the  $M1$  excitations in  $^{208}\text{Pb}$  calculated within the RenTBA with parametrization SKXm<sub>-0.49</sub> (red solid line) and within the RPA with parametrization SKXm<sub>-0.54</sub> (blue dashed line). The black dotted line represents the strength function (18) obtained from the experimental data [34, 35]. The smearing parameter  $\Delta = 20$  keV was used. See text for more details. Lower panel: the partial  $M1$  cross section  $\sigma_{M1}$  of the  $^{208}\text{Pb}(p, p')$  reaction from Ref. [39].

and  $\bar{E}_{>}$  are close to the experimental values, however the differences  $\Delta\bar{E} = \bar{E}_{>} - \bar{E}_{<}$  are different: the theoretical value  $\Delta\bar{E}_{\text{theor}} = 0.14$  MeV is less than the experimental one  $\Delta\bar{E}_{\text{exp}} = 0.31$  MeV by a factor of two. To estimate the fragmentation of the  $M1$  resonance we have also calculated the equivalent Gaussian width  $\Gamma$  in the interval 6.6–8.1 MeV both for the experimental and for the theoretical strength distributions. The results presented in last column of Table III show that the total width of the resonance is still underestimated.

Existence of the dip near the neutron separation energy in the experimental distribution of the  $M1$  strength in  $^{208}\text{Pb}$  is generally an uncertain point because the reliability of the experimental data [34, 35] goes down in this region. To some extent, the possible existence of this dip

is supported by the more recent data of the  $^{208}\text{Pb}(p, p')$  experiment [39]. The partial  $M1$  cross section  $\sigma_{M1}$  of this reaction is shown on the lower panel of Fig. 1. The dip in energy dependence of  $\sigma_{M1}$  near 7.4 MeV exists though it is less pronounced than for the strength function obtained from the data [34, 35]. Note, however, the following. First, the direct comparison of the  $M1$  strength functions  $S(E)$  and the cross section  $\sigma_{M1}(E)$  is hindered by the fact that they are determined by the different reaction mechanisms. The distribution of the  $B(M1)$  values can be obtained from the cross section of the  $(p, p')$  reaction only within the framework of some model assumptions, see, e.g., Ref. [40]. Second, the dip near 7.4 MeV is absent in the distribution of  $dB(M1)/dE$  deduced in [40] from the data of Ref. [39] and shown in Fig. 3(b) of Ref. [40]. But this fact can be explained by the different (and quite large) widths of the used energy bins that corresponds to the large and energy-dependent values of the smearing parameter  $\Delta$  of the strength function (18).

### V. THE FINE STRUCTURE OF THE $M1$ RESONANCE AND THE IMPACT OF THE SINGLE-PARTICLE CONTINUUM

To show the fine structure of the theoretical and experimental strength distributions and to study the role of the single-particle continuum (which in principle can manifest itself above the neutron separation energy) we have calculated the  $M1$  strength functions in  $^{208}\text{Pb}$  within the continuum RenTBA with  $\Delta = 1$  keV and 0.1 keV. The single-particle continuum was included within the response function formalism according to the method developed in Ref. [31]. In this approach the strength function  $S(E)$  is expressed through the response function, and the right-hand side of Eq. (18) is supplemented with the contribution of the continuum part of the spectrum. The parametrizations SKXm $_{-0.49}$  and SV-bas $_{-0.44}$  (the latter is discussed in more detail in Sec. VI) were used. The results for  $\Delta = 1$  keV are shown on the upper panel of Fig. 2 in terms of the function  $\tilde{B}_{M1}(E)$  defined as

$$\tilde{B}_{M1}(E) = \pi\Delta S(E). \quad (19)$$

Here we use this function because, as follows from Eq. (18),

$$B_\nu(M1) = \lim_{\Delta \rightarrow +0} \tilde{B}_{M1}(\omega_\nu). \quad (20)$$

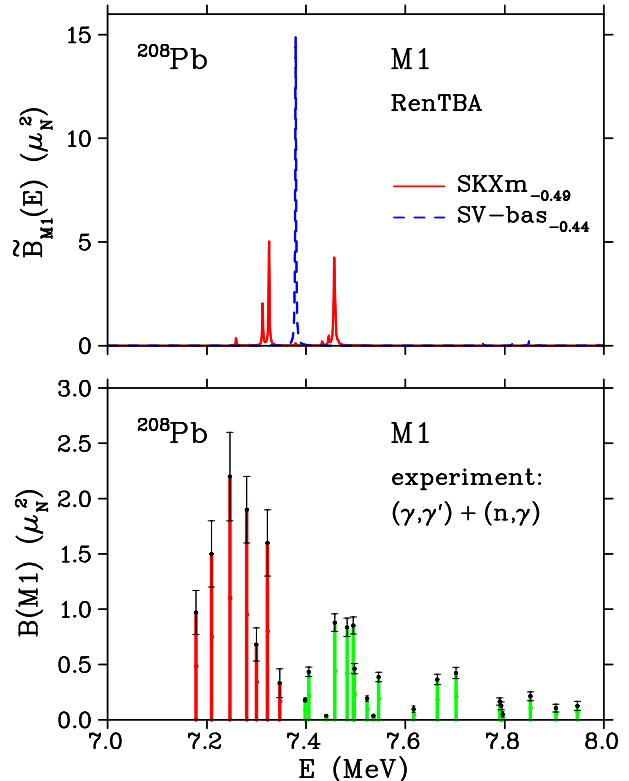


FIG. 2. Upper panel: strength distributions of the  $M1$  excitations in  $^{208}\text{Pb}$  calculated within the RenTBA with parametrizations SKXm $_{-0.49}$  (red solid line) and SV-bas $_{-0.44}$  (blue dashed line). The smearing parameter  $\Delta = 1$  keV was used. See text for more details. Lower panel: experimental distribution of the excitation probabilities  $B(M1)$  in  $^{208}\text{Pb}$  in the interval 7–8 MeV from Refs. [34] [ $^{208}\text{Pb}(\gamma, \gamma')$  reaction, red vertical lines] and [35] [ $^{207}\text{Pb}(n, \gamma)$  reaction, green vertical lines]. The error bars are indicated by the black lines.

So, if the  $\Delta$  is small, the peak values of the function  $\tilde{B}_{M1}(E)$  are close to the excitation probabilities at the peak energies. Note that Eq. (20) makes sense only for the states of the discrete spectrum. However, if the  $\Delta$  is greater than the escape width of the quasidecrete state in the continuum, the peak value of the function  $\tilde{B}_{M1}(E)$  allows us to estimate the integrated strength of the single resonance.

In the RenTBA calculation with the SKXm $_{-0.49}$  set and  $\Delta = 1$  keV, the fragmentation of two main peaks shown in Fig. 1 for the strength distributions with  $\Delta = 20$  keV is very small. This picture does not match the detailed fragmentation structure of the experimental distribution composed from data of Refs. [34, 35] and shown on the lower panel of Fig. 2. The  $M1$  strength in

the interval 7–8 MeV obtained in the RenTBA with the parametrization SV-bas<sub>-0.44</sub> is concentrated in one state without visible fragmentation, as in the case of the RPA.

The lack of fragmentation in the presented RenTBA calculations can be explained by the limited (though extended as compared to the RPA) kinds of the correlations included in the model. There are two natural generalizations of the RenTBA which enable one to include the additional correlations. First is the model taking into account the so-called ground-state correlations beyond the RPA. In Refs. [16, 17], it was shown that the inclusion of the correlations of this type increases the fragmentation of the  $M1$  resonance in  $^{208}\text{Pb}$ . The second generalization is the replacement of the intermediate  $1p1h \otimes$  phonon configurations by two-phonon configurations according to the scheme suggested in [41] and in analogy with the first versions of the quasiparticle-phonon model [42]. Note that the relative importance of these additional correlations increases at low energies due to the low level densities as compared to higher energies.

To analyze the effect of the single-particle continuum we first note that the theoretical neutron separation energies are equal to 7.30 MeV for the parametrization SKXm<sub>-0.49</sub> and 7.64 MeV for the parametrization SV-bas<sub>-0.44</sub>. So, the single peak of the RenTBA strength distribution for the SV-bas<sub>-0.44</sub> set shown on the upper panel of Fig. 2 (blue dashed line) is in the discrete spectrum, while the main strength of the distribution for the SKXm<sub>-0.49</sub> set (red solid line) lies in the continuum.

The effect of the continuum is determined by the values of the escape widths of the resonances. The full width at half maximum (FWHM) of the single peak of the strength distribution corresponding to the one or several overlapping resonances is formed by the escape and spreading widths and by the artificial width of  $2\Delta$  introduced by the smearing parameter. Thus, the FWHM can serve as an upper bound of the escape width. The distribution for the parametrization SKXm<sub>-0.49</sub> shown on the upper panel of Fig. 2 contains three main peaks with the energies 7.313 MeV, 7.325 MeV, and 7.457 MeV. These peaks correspond to four states of the discrete RenTBA spectrum with the energies 7.313 MeV, 7.326 MeV, 7.457 MeV, and 7.459 MeV which exhaust 92% of the summed strength of the  $M1$  resonance in the interval 6.6–8.1 MeV. So, we can confine ourselves to analyzing the widths of only these peaks. The respective values of the FWHM are equal to 2.1 keV for the quasidecrete states with  $E = 7.313$  MeV

and 7.325 MeV and to 3.4 keV for the resonance with  $E = 7.457$  MeV. The last FWHM value is appreciably greater than  $2\Delta$ . This is explained by the fact that the peak with  $E = 7.457$  MeV is formed by two overlapping resonances which correspond to two states of the discrete spectrum mentioned above.

In the calculation with  $\Delta = 0.1$  keV, the widths of the main peaks decrease. The values of the FWHM for the quasidecrete states with  $E = 7.313$  MeV and 7.325 MeV become less than 0.3 keV. The peak with  $E = 7.457$  MeV is split into two peaks separated by the small interval of 2 keV and having the widths which are less than 1 keV. Thus the escape widths of the main peaks of the distribution for the SKXm<sub>-0.49</sub> set are safely less than 1 keV. These results show that the inclusion of the single-particle continuum has no appreciable impact in the calculations with  $\Delta = 20$  keV presented in the paper.

## VI. THE PROBLEM OF THE FRAGMENTATION

The splitting of the isovector  $M1$  resonance in  $^{208}\text{Pb}$  into two main peaks obtained in RenTBA with the use of the parametrization SKXm<sub>-0.49</sub> is not a common result for the self-consistent calculations in our approach. In the typical case, if the EDF parameters  $g$  and  $g'$  are fitted to reproduce the experimental energy of the  $1_1^+$  state and the mean energy of the  $M1$  resonance in  $^{208}\text{Pb}$ , the fragmentation of the isovector  $M1$  resonance is reduced to the quenching of the main peak without appreciable broadening. This quenching is compensated by decreasing the renormalization constant  $\xi_s$  after which the forms of the RenTBA and RPA  $M1$  distributions become close to each other. This is illustrated in Fig. 3 where we show results for the modified SV-bas parametrizations.

To clarify the problem, we note that the effects of the fragmentation of the RPA states in TBA and RenTBA are determined by the energy-dependent induced interaction  $W(\omega)$ , Eq. (8a). The fragmentation of the RPA state with the energy  $\omega_{\text{RPA}}$  is strong if (i) one or more energies  $\Omega_c$  of the  $1p1h \otimes$  phonon configurations in Eqs. (8) are close to the shifted energy  $\tilde{\omega}_{\text{RPA}}$  (shifted due to the regular contribution of the remaining  $1p1h \otimes$  phonon configurations) and (ii) the respective amplitudes  $F_{ph}^{c(+)}$  are non-negligible. In the case of the nucleus  $^{208}\text{Pb}$ , the isovector  $M1$  strength in the RPA is concentrated as a rule in one state with the energy  $\omega_{\text{RPA}}(1_2^+)$  (the  $1_1^+$  RPA

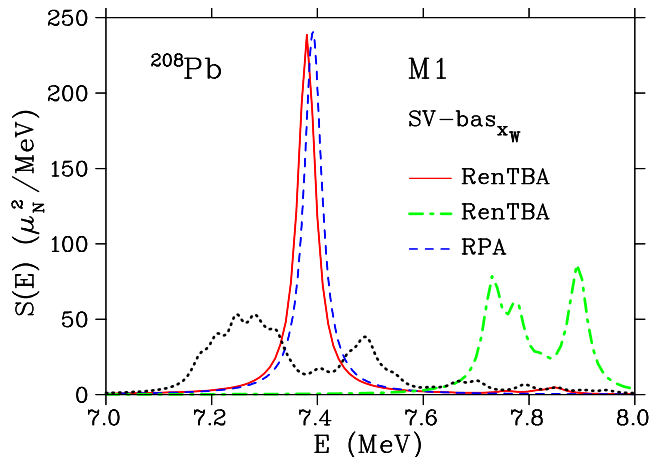


FIG. 3. Strength distributions of the  $M1$  excitations in  $^{208}\text{Pb}$  calculated within the RenTBA with parametrizations SV-bas $_{-0.44}$  (red solid line) and SV-bas' $_{-0.44}$  (green dashed-dotted line) and within the RPA with parametrization SV-bas $_{-0.50}$  (blue dashed line) in comparison with the experiment (black dotted line). The smearing parameter  $\Delta = 20$  keV was used. See text for more details.

state is isoscalar) which is formed by two  $1p1h$  configurations:  $\pi(1h_{9/2} \otimes 1h_{11/2}^{-1})$  and  $\nu(1i_{11/2} \otimes 1i_{13/2}^{-1})$ . So, the  $ph$  indices of the amplitudes  $F_{ph}^{c(+)}$  producing appreciable fragmentation of the  $1_2^+$  RPA state should be one of these two combinations. Under this condition and according to the selection rules for the  $M1$  excitations, the minimum value of  $\Omega_c$  in  $^{208}\text{Pb}$  is determined by the configuration  $c = \{\pi(1h_{9/2} \otimes 3s_{1/2}^{-1}) \otimes 5_1^-\}$ , that is

$$\Omega_c^{\min} = \varepsilon_{ph}^{\pi} + \omega(5_1^-), \quad (21a)$$

where

$$\varepsilon_{ph}^{\pi} = \varepsilon_p^{\pi}(1h_{9/2}) - \varepsilon_h^{\pi}(3s_{1/2}). \quad (21b)$$

It turns out that for most Skyrme EDF parametrizations the value of  $\Omega_c^{\min}$  is substantially greater than the mean energy of the isovector  $M1$  resonance in  $^{208}\text{Pb}$ , that is  $\Omega_c^{\min} > 7.4$  MeV. Thus, if the parameters of the EDF are fitted to reproduce this mean energy, the fragmentation of the isovector  $M1$  resonance is reduced to its quenching as mentioned above. The parametrization SKXm $_{-0.49}$  is an exception because the value of  $\omega_{\text{RenTBA}}(5_1^-)$  comes close the experimental value which, in turn, yields an  $\Omega_c^{\min}$  close to 7.4 MeV. This is shown in Table IV in comparison with the case of the SV-bas $_{-0.44}$  parametrization.

TABLE IV. The values of the particle-hole energies  $\varepsilon_{ph}^{\pi} = \varepsilon_p^{\pi}(1h_{9/2}) - \varepsilon_h^{\pi}(3s_{1/2})$ , the energies of  $5_1^-$  phonon, and their sums  $\Omega_c^{\min}$ , Eqs. (21), in the RenTBA for the parametrizations SKXm $_{-0.49}$  and SV-bas $_{-0.44}$ . The experimental values are given in the last line.

EDF	$\varepsilon_{ph}^{\pi}$ (MeV)	$\omega(5_1^-)$ (MeV)	$\Omega_c^{\min}$ (MeV)
SKXm $_{-0.49}$	4.14	3.24	7.38
SV-bas $_{-0.44}$	4.27	3.55	7.82
experiment	4.21	3.20	7.41

Note that the splitting of the isovector  $M1$  resonance shown in Fig. 1 is achieved only in the RenTBA. In conventional TBA, the energies of the phonons in Eqs. (8) are calculated within the RPA. In the case of the parametrization SKXm $_{-0.49}$ , the energy  $\omega_{\text{RPA}}(5_1^-) = 3.64$  MeV that increases the energy  $\Omega_c^{\min}$  and leads to the RPA-like result in the TBA similar to shown in Fig. 3 by the red solid line.

On the other hand, the fragmentation of the isovector  $M1$  resonance in  $^{208}\text{Pb}$  in itself can be obtained also in the case  $\Omega_c^{\min} > 7.4$  MeV if the isovector  $M1$  strength is shifted to higher energies by increasing the EDF parameter  $g'$ . This is shown in Fig. 3 for the parametrization SV-bas' $_{-0.44}$  which is constructed from the set SV-bas $_{-0.44}$  by changing the parameter  $g'$  from 1.03 for SV-bas $_{-0.44}$  to 1.46 for SV-bas' $_{-0.44}$  (however, the set of the phonons in this illustrative RenTBA calculation for SV-bas' $_{-0.44}$  was used the same as for SV-bas $_{-0.44}$ ). Thus, the simultaneous description of the mean energy of the isovector  $M1$  resonance in  $^{208}\text{Pb}$  and of the fragmentation of this resonance in the self-consistent calculation is seemingly possible only in rare circumstances as, e.g., in case of the parametrization SKXm $_{-0.49}$ .

Note that the fragmentation of the isovector  $M1$  resonance in  $^{208}\text{Pb}$  was obtained in the early calculations within the shell model in the  $1p1h + 2p2h$  space [9] and within the models based on the TFFS [8] and including the particle-phonon interaction on top of the RPA (see, e.g., [10, 11, 14, 16, 17]). This result is explained by two reasons. First, the mean energy of the isovector  $M1$  resonance in these calculations was greater than the experimental value. The shift to higher energies increases the spreading of the  $M1$  strength as was noted in Ref. [9] and is demonstrated in Fig. 3. Second, the phonon energies in the calculations of Refs. [11, 14, 16, 17] were fitted to their experimental values that makes the value



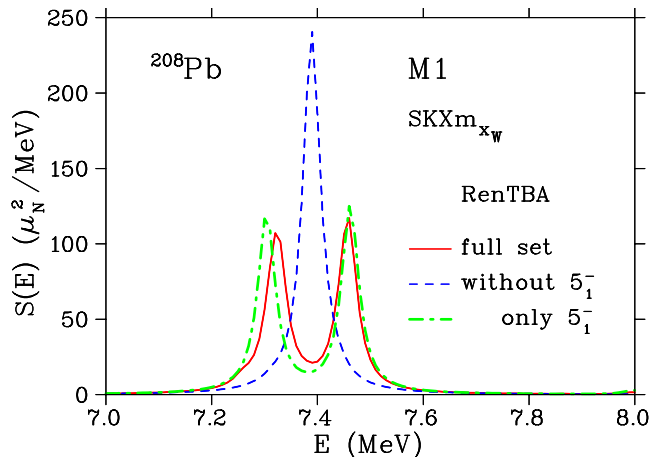


FIG. 4. Strength distributions of the  $M1$  excitations in  $^{208}\text{Pb}$  calculated within the RenTBA with the full set of the phonons and with parametrization SKXm $_{-0.49}$  (red solid line), with the set of all the phonons except for the  $5_1^-$  phonon and with parametrization SKXm' $_{-0.49}$  (blue dashed line) and with the set of the phonons including only the  $5_1^-$  phonon and with parametrization SKXm'' $_{-0.49}$  (green dashed-dotted line). The smearing parameter  $\Delta = 20$  keV was used. See text for more details.

of  $\Omega_c^{\min}$  more close to the mean energy of the isovector  $M1$  resonance, see Table IV.

To demonstrate the role of the intermediate  $1p1h \otimes \text{phonon}$  configuration  $\pi(1h_{9/2} \otimes 3s_{1/2}^{-1}) \otimes 5_1^-$  in the effect of the fragmentation under discussion we show in Fig. 4 the results of three RenTBA calculations with the use of parametrizations SKXm $_{-0.49}$ , SKXm' $_{-0.49}$ , and SKXm'' $_{-0.49}$  (see Table II). The RenTBA calculation with the use of parametrization SKXm $_{-0.49}$  coincides with one shown in Fig. 1. In the calculation with the use of SKXm' $_{-0.49}$ , the  $5_1^-$  phonon was excluded and the EDF parameter  $g'$  was slightly changed to fit the mean energy of the isovector  $M1$  resonance to the experiment. The calculation with SKXm'' $_{-0.49}$  represents the opposite case: only the  $5_1^-$  phonon was included in the phonon basis of the RenTBA and the EDF parameters  $g$  and  $g'$  were changed to fit the energy of the  $1_1^+$  state and the mean energy of the isovector  $M1$  resonance to the experiment. The renormalization constant  $\xi_s$  was also changed to compensate decreasing of the quenching of the  $M1$  strength. However, the characteristics of the same phonons (energies, etc.) were the same in all three calculations. These results show

that the splitting of the isovector  $M1$  resonance in  $^{208}\text{Pb}$  is determined in the considered model practically exclusively by the configuration  $\pi(1h_{9/2} \otimes 3s_{1/2}^{-1}) \otimes 5_1^-$ . The other  $1p1h \otimes \text{phonon}$  configurations produce only the shift of the  $M1$  resonance and the quenching of the  $M1$  strength.

## VII. RESULTS FOR THE LOW-ENERGY ELECTRIC EXCITATIONS IN $^{208}\text{Pb}$

In section VI, we have shown that the RenTBA using the modified Skyrme EDF SKXm $_{-0.49}$  gives an energy of the first  $5^-$  state in  $^{208}\text{Pb}$  close to its experimental value. Here we consider the results of the RenTBA and RPA calculations for the first excited states of natural parity in  $^{208}\text{Pb}$  with the multipolarity  $L$  from 2 to 6 both for the SKXm $_{-0.49}$  and the SV-bas $_{-0.44}$  parametrizations. The results are presented in Tables V and VI. Note that the

TABLE V. The energies (in MeV) of the first excited states of the natural parity in  $^{208}\text{Pb}$  calculated within the RenTBA and the RPA with the use of the modified Skyrme EDFs SKXm $_{-0.49}$  and SV-bas $_{-0.44}$ . The experimental data are taken from Ref. [43].

$L^\pi$	SKXm $_{-0.49}$		SV-bas $_{-0.44}$		experiment
	RenTBA	RPA	RenTBA	RPA	
$2_1^+$	4.01	4.45	4.00	4.42	4.09
$3_1^-$	2.69	2.91	2.88	3.10	2.61
$4_1^+$	4.29	4.81	4.30	4.80	4.32
$5_1^-$	3.19	3.64	3.49	3.93	3.20
$6_1^+$	4.43	5.02	4.53	5.13	4.42

RenTBA results have been obtained without use of the diagonal approximation which is used in the model only for the phonons entering the intermediate  $1p1h \otimes \text{phonon}$  configurations. It explains the small difference between the energies of the  $5_1^-$  state listed in Tables IV (where the diagonal approximation is used) and V.

The RenTBA energies calculated with the parametrization SKXm $_{-0.49}$  agree fairly well with the experiment. The deviations for SV-bas $_{-0.44}$  are slightly greater (except for the  $4_1^+$  state). The RPA gives too large energies for both parametrizations. The energy shift  $\omega(\text{RPA}) - \omega(\text{RenTBA})$  is between 0.2 MeV for the  $3_1^-$  state and 0.6 MeV for the  $6_1^+$  state.

The situation is the opposite for the excitation probabilities shown in Table VI. The RPA results are closer to the experiment as compared to the RenTBA results

TABLE VI. The same as in Table V but for the excitation probabilities  $B(EL)$  (in units of  $e^2\text{fm}^{2L}$ ).

$L^\pi$	SKXm <sub>-0.49</sub>		SV-bas <sub>-0.44</sub>		experiment
	RenTBA	RPA	RenTBA	RPA	
$2_1^+$	$2.6 \times 10^3$	$3.2 \times 10^3$	$2.5 \times 10^3$	$3.0 \times 10^3$	$3.2 \times 10^3$
$3_1^-$	$5.6 \times 10^5$	$6.4 \times 10^5$	$5.8 \times 10^5$	$6.4 \times 10^5$	$6.1 \times 10^5$
$4_1^+$	$1.1 \times 10^7$	$1.5 \times 10^7$	$9.6 \times 10^6$	$1.3 \times 10^7$	$1.6 \times 10^7$
$5_1^-$	$1.9 \times 10^8$	$2.9 \times 10^8$	$2.3 \times 10^8$	$3.6 \times 10^8$	$4.5 \times 10^8$
$6_1^+$	$2.6 \times 10^{10}$	$3.6 \times 10^{10}$	$1.4 \times 10^{10}$	$2.2 \times 10^{10}$	$6.7 \times 10^{10}$

(and are in a good agreement with the experiment for  $2_1^+$ ,  $3_1^-$ , and  $4_1^+$  states). The decrease of the  $B(EL)$  values in RenTBA is caused by the quenching as in the case of the  $M1$  excitations.

By construction, the modified parametrizations SKXm<sub>-0.49</sub> and SV-bas<sub>-0.44</sub> describe the nuclear ground-state properties within the Skyrme EDF approach (with approximately the same accuracy as the original parametrizations SKXm and SV-bas) and reproduce the basic experimental characteristics of the  $M1$  excitations in  $^{208}\text{Pb}$  within the RenTBA. The results of this section show that the RenTBA with the use of these modified parametrizations is applicable also to the description of the low-energy electric excitations in this nucleus.

## VIII. CONCLUSIONS

The present paper is a continuation of our recent work [23] in which we investigated the low-energy  $M1$  excitations in  $^{208}\text{Pb}$  within the self-consistent RPA based on the Skyrme energy-density functionals (EDF). Here

we use the extended self-consistent model including the particle-phonon coupling within the renormalized time blocking approximation (RenTBA, [25]). As in the case of the self-consistent RPA, the description of the basic experimental characteristics of the  $M1$  excitations in  $^{208}\text{Pb}$  (energy and strength of the  $1_1^+$  state as well as mean energy and summed strength of the isovector  $M1$  resonance) requires refitting some of the spin-related parameters of the Skyrme EDF within the self-consistent RenTBA. We have determined several sets of these parameters from this condition. It has been shown that the observed fragmentation of the isovector  $M1$  resonance in  $^{208}\text{Pb}$  which is absent in all the RPA calculations can be to a certain extent described within the self-consistent RenTBA. However, this description is not fully quantitative and is attained only in some cases of the modified functionals of the Skyrme type. We have found that the necessary condition to obtain this fragmentation in our model is the proximity of the energy of the intermediate  $1p1h \otimes$  phonon configuration  $\pi(1h_{9/2} \otimes 3s_{1/2}^{-1}) \otimes 5_1^-$  to the mean energy of the isovector  $M1$  resonance in  $^{208}\text{Pb}$ , i.e. the proximity of the energy of  $5_1^-$  phonon to the experimental excitation energy of the  $5_1^-$  state in  $^{208}\text{Pb}$ . We have also shown that the modified parametrizations of the Skyrme EDF presented in the paper can be used in the description of the low-energy electric excitations within the RenTBA.

## ACKNOWLEDGMENTS

V.T. is grateful to Prof. V.Yu. Ponomarev for discussions. Research was carried out using computational resources provided by Resource Center ‘‘Computer Center of SPbU’’.

- 
- |   |  |
|---|--|
| <p>[1] R. M. Laszewski, R. Alarcon, D. S. Dale, and S. D. Hoblit, Phys. Rev. Lett. <b>61</b>, 1710 (1988).</p> <p>[2] S. Kamedzhiev, J. Speth, and G. Tertychny, Phys. Rep. <b>393</b>, 1 (2004).</p> <p>[3] J. D. Vergados, Phys. Lett. B <b>36</b>, 12 (1971).</p> <p>[4] P. Ring and J. Speth, Phys. Lett. B <b>44</b>, 477 (1973).</p> <p>[5] V. N. Tkachev, I. N. Borzov, and S. P. Kamedzhiev, Sov. J. Nucl. Phys. <b>24</b>, 373 (1976).</p> <p>[6] J. Speth, V. Klemt, J. Wambach, and G. E. Brown, Nucl. Phys. A <b>343</b>, 382 (1980).</p> <p>[7] I. N. Borzov, S. V. Tolokonnikov, and S. A. Fayans, Sov. J. Nucl. Phys. <b>40</b>, 732 (1984).</p> | <p>[8] A. B. Migdal, <i>Theory of Finite Fermi Systems and Application to Atomic Nuclei</i> (Wiley, New York, 1967).</p> <p>[9] T.-S. H. Lee and S. Pittel, Phys. Rev. C <b>11</b>, 607 (1975).</p> <p>[10] J. S. Dehesa, J. Speth, and A. Faessler, Phys. Rev. Lett. <b>38</b>, 208 (1977).</p> <p>[11] S. P. Kamedzhiev and V. N. Tkachev, Phys. Lett. B <b>142</b>, 225 (1984).</p> <p>[12] D. Cha, B. Schwesinger, J. Wambach, and J. Speth, Nucl. Phys. A <b>430</b>, 321 (1984).</p> <p>[13] D. T. Khoa, V. Y. Ponomarev, and A. I. Vdovin, Preprint JINR <b>E4-86-198</b> (1986).</p> |
|---|--|

- [14] S. P. Kamerdzhiev and V. N. Tkachev, *Z. Phys. A* **334**, 19 (1989).
- [15] V. I. Tselyaev, *Sov. J. Nucl. Phys.* **50**, 780 (1989).
- [16] S. P. Kamerdzhiev and V. I. Tselyaev, *Bull. Acad. Sci. USSR, Phys. Ser.* **55**, 45 (1991).
- [17] S. P. Kamerdzhiev, J. Speth, G. Tertychny, and J. Wambach, *Z. Phys. A* **346**, 253 (1993).
- [18] L.-G. Cao, G. Colò, H. Sagawa, P. F. Bortignon, and L. Sciacchitano, *Phys. Rev. C* **80**, 064304 (2009).
- [19] P. Vesely, J. Kvasil, V. O. Nesterenko, W. Kleinig, P.-G. Reinhard, and V. Y. Ponomarev, *Phys. Rev. C* **80**, 031302(R) (2009).
- [20] V. O. Nesterenko, J. Kvasil, P. Vesely, W. Kleinig, P.-G. Reinhard, and V. Y. Ponomarev, *J. Phys. G: Nucl. Part. Phys.* **37**, 064034 (2010).
- [21] L.-G. Cao, H. Sagawa, and G. Colò, *Phys. Rev. C* **83**, 034324 (2011).
- [22] P. Wen, L.-G. Cao, J. Margueron, and H. Sagawa, *Phys. Rev. C* **89**, 044311 (2014).
- [23] V. Tselyaev, N. Lyutorovich, J. Speth, P.-G. Reinhard, and D. Smirnov, *Phys. Rev. C* **99**, 064329 (2019).
- [24] M. Bender, P.-H. Heenen, and P.-G. Reinhard, *Rev. Mod. Phys.* **75**, 121 (2003).
- [25] V. Tselyaev, N. Lyutorovich, J. Speth, and P.-G. Reinhard, *Phys. Rev. C* **97**, 044308 (2018).
- [26] C. Toepffer and P.-G. Reinhard, *Ann. Phys. (N.Y.)* **181**, 1 (1988).
- [27] K. Gütter, P.-G. Reinhard, K. Wagner, and C. Toepffer, *Ann. Phys. (N.Y.)* **225**, 339 (1993).
- [28] V. I. Tselyaev, *Phys. Rev. C* **88**, 054301 (2013).
- [29] N. Lyutorovich, V. Tselyaev, J. Speth, S. Krewald, F. Grümmer, and P.-G. Reinhard, *Phys. Lett. B* **749**, 292 (2015).
- [30] N. Lyutorovich, V. Tselyaev, J. Speth, S. Krewald, and P.-G. Reinhard, *Phys. At. Nucl.* **79**, 868 (2016).
- [31] V. Tselyaev, N. Lyutorovich, J. Speth, S. Krewald, and P.-G. Reinhard, *Phys. Rev. C* **94**, 034306 (2016).
- [32] B. A. Brown, *Phys. Rev. C* **58**, 220 (1998).
- [33] P. Klüpfel, P.-G. Reinhard, T. J. Bürvenich, and J. A. Maruhn, *Phys. Rev. C* **79**, 034310 (2009).
- [34] T. Shizuma, T. Hayakawa, H. Ohgaki, T. Toyokawa, T. Komatsubara, N. Kikuzawa, A. Tamii, and H. Nakada, *Phys. Rev. C* **78**, 061303(R) (2008).
- [35] R. Köhler, J. A. Wartena, H. Weigmann, L. Mewissen, F. Poortmans, J. P. Theobald, and S. Raman, *Phys. Rev. C* **35**, 1646 (1987).
- [36] P.-G. Reinhard and H. Flocard, *Nucl. Phys. A* **584**, 467 (1995).
- [37] M. M. Sharma, G. Lalazissis, J. König, and P. Ring, *Phys. Rev. Lett.* **74**, 3744 (1995).
- [38] E. Chabanat, P. Bonche, P. Haensel, J. Meyer, and R. Schaeffer, *Nucl. Phys. A* **635**, 231 (1998).
- [39] I. Poltoratska, P. von Neumann-Cosel, A. Tamii, T. Adachi, C. A. Bertulani, J. Carter, M. Dozono, H. Fujita, K. Fujita, Y. Fujita, K. Hatanaka, M. Itoh, T. Kawabata, Y. Kalmykov, A. M. Krumbholz, E. Litvinova, H. Matsubara, K. Nakanishi, R. Neveling, H. Okamura, H. J. Ong, B. Özel-Tashenov, V. Y. Ponomarev, A. Richter, B. Rubio, H. Sakaguchi, Y. Sakemi, Y. Sasamoto, Y. Shimbara, Y. Shimizu, F. D. Smit, T. Suzuki, Y. Tameshige, J. Wambach, M. Yosoi, and J. Zenihiro, *Phys. Rev. C* **85**, 041304(R) (2012).
- [40] J. Birkhan, H. Matsubara, P. von Neumann-Cosel, N. Pietralla, V. Y. Ponomarev, A. Richter, A. Tamii, and J. Wambach, *Phys. Rev. C* **93**, 041302(R) (2016).
- [41] V. I. Tselyaev, *Phys. Rev. C* **75**, 024306 (2007).
- [42] V. G. Soloviev, *Theory of Atomic Nuclei: Quasiparticles and Phonons* (Institute of Physics, Bristol and Philadelphia, 1992).
- [43] M. Martin, *Nuclear Data Sheets* **108**, 1583 (2007).